FINAL REPORT

CONTRACT F61775-99-WE004

"SIMULATION OF LOW LIGHT LEVEL ADAPTIVE OPTICS SYSTEMS"

DR. C. J. SOLOMON

UNIVERSITY OF KENT
CANTERBURY, UK

JUNE 2000

REPORT DOCUMENTATION PAGE

Form Approved OMB No. 0704-0188

1. AGENCY USE ONLY (Leave blank)	2. REPORT DATE	3. REPORT TYPE AND DATES COVERED
	28-June-2000	Final Report

4. TITLE AND SUBTITLE

~~Optimization~~ Of Low-Light-Level Adaptive Optics Systems
Simulation

5. FUNDING NUMBERS

F61775-99-WE004

6. AUTHOR(S)

Dr. Christopher J. Solomon

7. PERFORMING ORGANIZATION NAME(S) AND ADDRESS(ES)

University of Kent
Canterbury CT2 7NR
United Kingdom

8. PERFORMING ORGANIZATION REPORT NUMBER

N/A

9. SPONSORING/MONITORING AGENCY NAME(S) AND ADDRESS(ES)

EOARD
PSC 802 BOX 14
FPO 09499-0200

10. SPONSORING/MONITORING AGENCY REPORT NUMBER

SPC 99-4004

11. SUPPLEMENTARY NOTES

12a. DISTRIBUTION/AVAILABILITY STATEMENT

Approved for public release; distribution is unlimited.

12b. DISTRIBUTION CODE

A

13. ABSTRACT (Maximum 200 words)

This report results from a contract tasking University of Kent as follows: The contractor will provide documentation for the computer program developed in contract F61775-98-WE079, and develop optimum adaptive optic designs for low-light-level applications that will handle generation of time-evolving turbulent wavefronts, adjustment of wind speed of the turbulent layers, adjustment of key observational parameters such as the iso-planatic patch size, and the ability to evaluate match filtering techniques for reducing mean-square residual wavefront error.

14. SUBJECT TERMS

EOARD, Modelling & Simulation, Adaptive Optics, Atmospheric Propagation

15. NUMBER OF PAGES

25

16. PRICE CODE

N/A

17. SECURITY CLASSIFICATION OF REPORT	18. SECURITY CLASSIFICATION OF THIS PAGE	19. SECURITY CLASSIFICATION OF ABSTRACT	20. LIMITATION OF ABSTRACT
UNCLASSIFIED	UNCLASSIFIED	UNCLASSIFIED	UL

SPC 99-4004 –"Simulation of low light level adaptive optics systems"

Final report –June 2000

Dr C.J. Solomon

ABSTRACT

This report addresses the development of simulation tools which are suitable for the design and analysis of optimum imaging scenarios for adaptive optics systems. In particular, we discuss the physical basis and suitability of the modular CAOS system for such studies. A description of its essential features and the basic philosophy behind its use is included together with an illustrative design. Summary documentation is also included. We conclude that CAOS is a powerful system with considerable flexibility and possessing considerable potential for adaptive optics study and analysis.

A second part of the report is given in the form of a paper submitted June 8th 2000 to Journal of the Optical Society of America A – "Variational solution for modal wavefront projection functions of minimum error norm". This describes the derivation of vector functions which are orthogonal to the gradients of the wavefront modes. Their property of minimum noise propagation allows an optimal method for estimating atmospherically distorted wavefronts through direct integration of the wavefront slope measurements.

INTRODUCTION

Adaptive optics (AO) systems require a sufficiently bright reference source to enable adequate measurement of the wavefront aberrations. This is the fundamental limit on the ability to achieve good correction. The lack of enough bright natural guide stars (NGS) close to a faint scientific object (within the isoplanatic patch) limits the sky coverage of AO systems. A solution, (first proposed in the open literature by Foy & Labeyrie, [1]) is to use a laser beam to create a so-called laser guide star (LGS) or laser beacon. Two types of LGS can be considered: one exploits Rayleigh-Mie scattering in the first 10-20 km of the atmosphere [2], the other takes advantage of the resonant scattering by sodium atoms at approximately 90 km altitude [3,4].

Both solutions have in fact produced a variety of new problems. In particular, the finite altitude of the artificial star (the so-called cone effect [5]) and the blindness to the tip-tilt modes of the wavefront (tip-tilt indeterminacy [6]) are major considerations. The cost of such systems is also considerable. AO systems which will employ LGS must therefore be efficiently implemented. Another topic of quite general interest in AO relates to the optimal use of the incoming photon flux. One is rarely afforded the luxury of high signal-noise ratios and this implies an ongoing interest in the study of innovative wavefront sensing techniques. Optimal use of the available photon flux would allow us to increase the limiting magnitude of NGS AO (increasing the sky coverage) or to reduce the necessary laser power. For these applications and others a powerful, realistic and versatile simulation tool is desirable.

1.1 CAOS

CAOS (Code for adaptive optics systems) is a purpose-designed software tool for the simulation of adaptive optics systems. Written in the IDL programming language, there have been a number of contributors and CAOS is freely available to workers in adaptive optics. The development of CAOS came from a need to provide reliable and comprehensive software for AO simulation to a growing number of workers in the community. As of June 2000, CAOS 2.0 has been released and the software seems likely to see further development and revision in the future. The code has two principal aims. The first is to accurately simulate real AO systems in order to evaluate and characterize system performance. The second is to allow the evaluation of new techniques, designs and studies.

1.2 Features of CAOS

CAOS has two key features which make it easy to use –

- A modular structure
- A graphical application builder

1.2.1 Modules

Modules are the basic building blocks of the simulation. Each module corresponds to a particular identifiable aspect of the adaptive optics system or the interpretation of its results. Chaos in version 2.0 has the following modules-

Atmospheric building	ATM
Beam splitter	BSP

Centroiding calculus	CEN
Calibration fibre	CFB
Command sequencer	CSQ
Data display	DIS
Geometrical propagation	DMI
interferometric beam combiner	IBC
Imaging device	IMG
Laser definition	LAS
Make calibration data	MCA
Sodium layer	NLS
Wavefront reconstruction	REC
Data saving	SAV
Shack Hartmann sensor	SHS
Source definition	SRC
Structure function calculus	STF
Tip -tilt centroiding	TCE
Time filtering	TFL
Tip-tilt Mirror	TTM
Wavefront adding	WFA

Details of some of the most important modules are given later in the report.

1.2.2 Philosophy of CAOS

Each module is defined by a standard group of function calls, a set of parameters which are required for the module's correct execution and a set of predetermined inputs and outputs.

The basic philosophy is that the user *not be required to perform any coding* but need only combine the modules in a meaningful way and supply meaningful values of the parameters to each of the modules. In this way, and within the constraints imposed by the software, the designer may concentrate on the concepts. To assist with this simulation design, a graphical interface (gui) termed the *application builder* is supplied.

1.3 The application builder (AB)

The application builder is a graphical tool provided to aid the design of simulation programs. It is used only during the design phase. After that the simulation program will run as a stand-alone application with no subsequent interaction with the AB.

A schematic diagram of an arbitrary simulation program designed via the AB, together with the module list scroll-down menu of the AB, is shown in Fig. 1. The simple interface consists of a *worksheet* - essentially a collection of contiguous cells – with some pull-down menus. Each cell in the worksheet may accomodate a *module*.

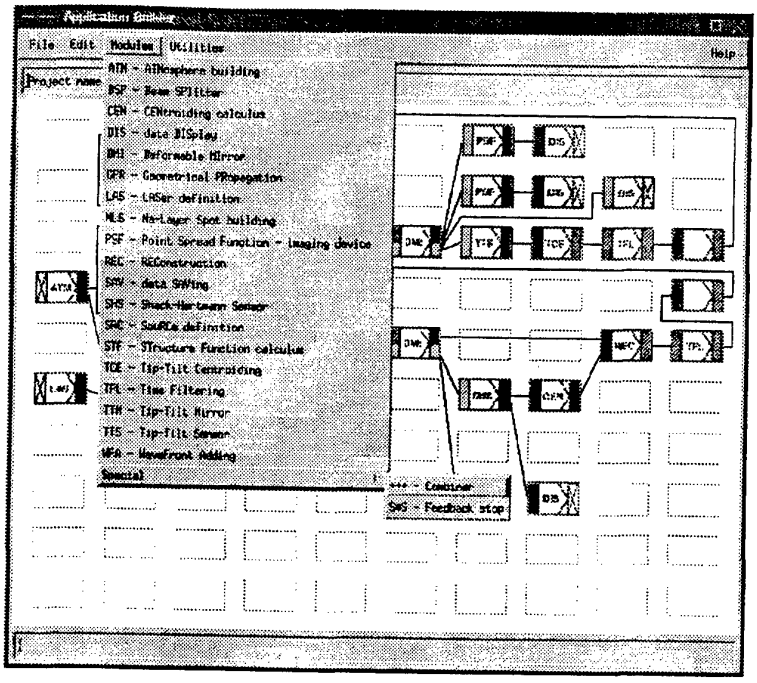

Figure 1: CAOS Worksheet with pull-down menus

Essentially, modules are selected from the pull-down "Modules" menu and dropped into a chosen cell position on the worksheet. From the point of view of the application builder, each module can only be executed if the required set of inputs to the module are available. These inputs are generally provided by the outputs of other modules. Accordingly, the input and output ends of each module are colour coded to indicate compatibility. The basic appearance of a module as it appears on the worksheet is given below in figure 2.

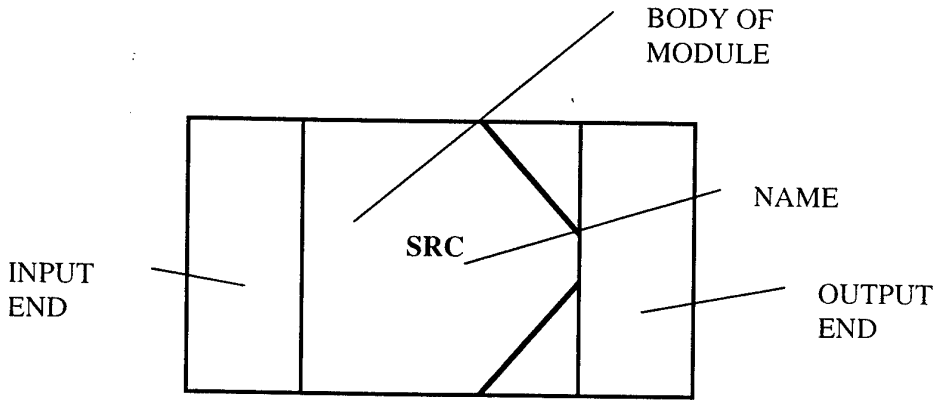

Figure 2: Simulation Module

The colour of the input and output simply specifies compatibility between modules. These cannot be changed or edited. Each output may be joined to an arbitrary number of input handles but

input handles may only receive a single link from an output handle. Conceptually speaking, the *body* of the module contains the parameters which are required for the module to execute once the design is complete. These can be set and edited by clicking with the mouse on the body of the module and this invokes the corresponding "parameter setting" GUI - i.e. a graphical window containing the current values of the required parameters as editable text fields.

Links are then defined between the output of a given module and the input of another thus defining the data flow within a simulation project. In the simple example below in figure 3, we see the source module (which defines the type of luminous object we are looking at) and the atmospheric builder module being linked with the geometric propagation module. In this particular case, these three modules would be suitable to simulate the propagation of the wavefront from a chosen source through an atmosphere of selected spatiotemporal behaviour to the pupil plane of the telescope.

FIG.3 LINKING MODULES

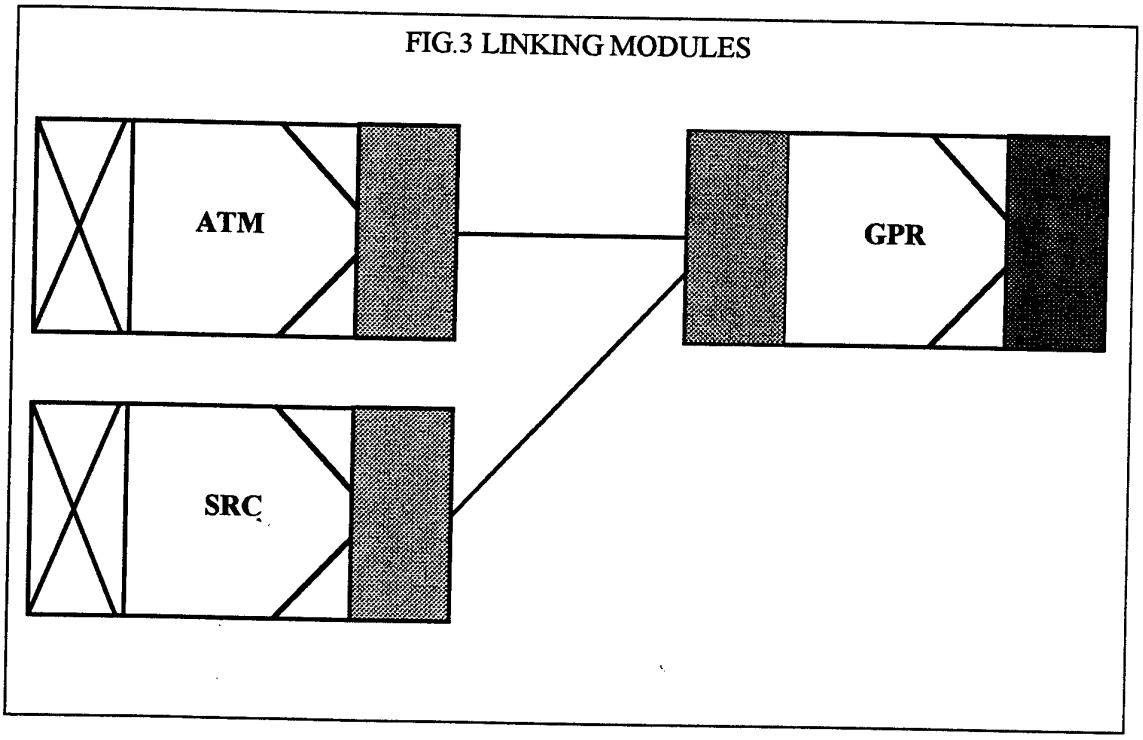

Note that the output colour of each module in the sequence matches the input colour. Grey is used to indicate compatibility with all modules. Cross-hatching at the input indicates that no other modules may feed into the given module.

The links (indicated in this case simply by straight lines) are made by clicking on the output of one module with the mouse followed by clicking on the input of the other.

After the design is completed, the block diagram of linked modules is analysed by the application builder and the IDL code implementing the simulation program is generated. The whole simulation can be saved as a project which may be executed and opened for later modification if desired.

1.4 CAOS Design – basic summary

In summary, the simulation design procedure may be reduced to the following sequence –

TASK	ACTION
Select required modules	From pull-down menu in the application builder, select and drop modules into cells on worksheet
Specify the values of the parameters required by each module	Click on body of selected module to invoke GUI parameter setting window. Set parameter values and save
Form legal links between modules	Click on the output end of module A followed by a click on the input end of module B. This links A and B
Save project	Select from pull-down menu

1.5 Running CAOS simulations

CAOS simulations are run as normal IDL projects from the command line IDL interface. Any inconsistencies in the parameter setting of each module are normally detected prior to this stage by the application builder which will indicate where the inconsistency has occurred and suggest alternative values.

1.6 Platform dependence, reliability and bugs

CAOS has been primarily developed to run on a UNIX/LINUX platform. As freeware, the developers make no assurances as to reliability and existence of bugs. The reliability of CAOS linux v2.0 is however considerably better than previous version. CAOS 2.0 for MsWindows95-98 exists but reliability is currently not as good.

1.7 Obtaining CAOS

Scientific workers who wish to use CAOS should mail marcel@arcetri.astro.it. On receiving permission, they may then download the software from the corresponding ftp site.

1.8 EXAMPLE APPLICATION

In this section, simply to illustrate the concept more clearly, we present a conceptual design and result obtained from a relatively complex LGS adaptive optics system. Full details are available in the reference [7] . Figure 4 shows the conceptual design of the system in which the modules are placed on the worksheet and then linked in the appropriate configuration.

In the scenario depicted in fig 4, a natural guide star is used to sense and correct the tip-tilt modes of the atmosphere whilst a laser beacon is used to correct the higher order aberrations using a Shack-Hartmann sensor. In this particular study, two equal turbulent layers at 0 and 10 km altitude with 4m/s and 8m/s wind speed perpendicular to each other, were defined within the

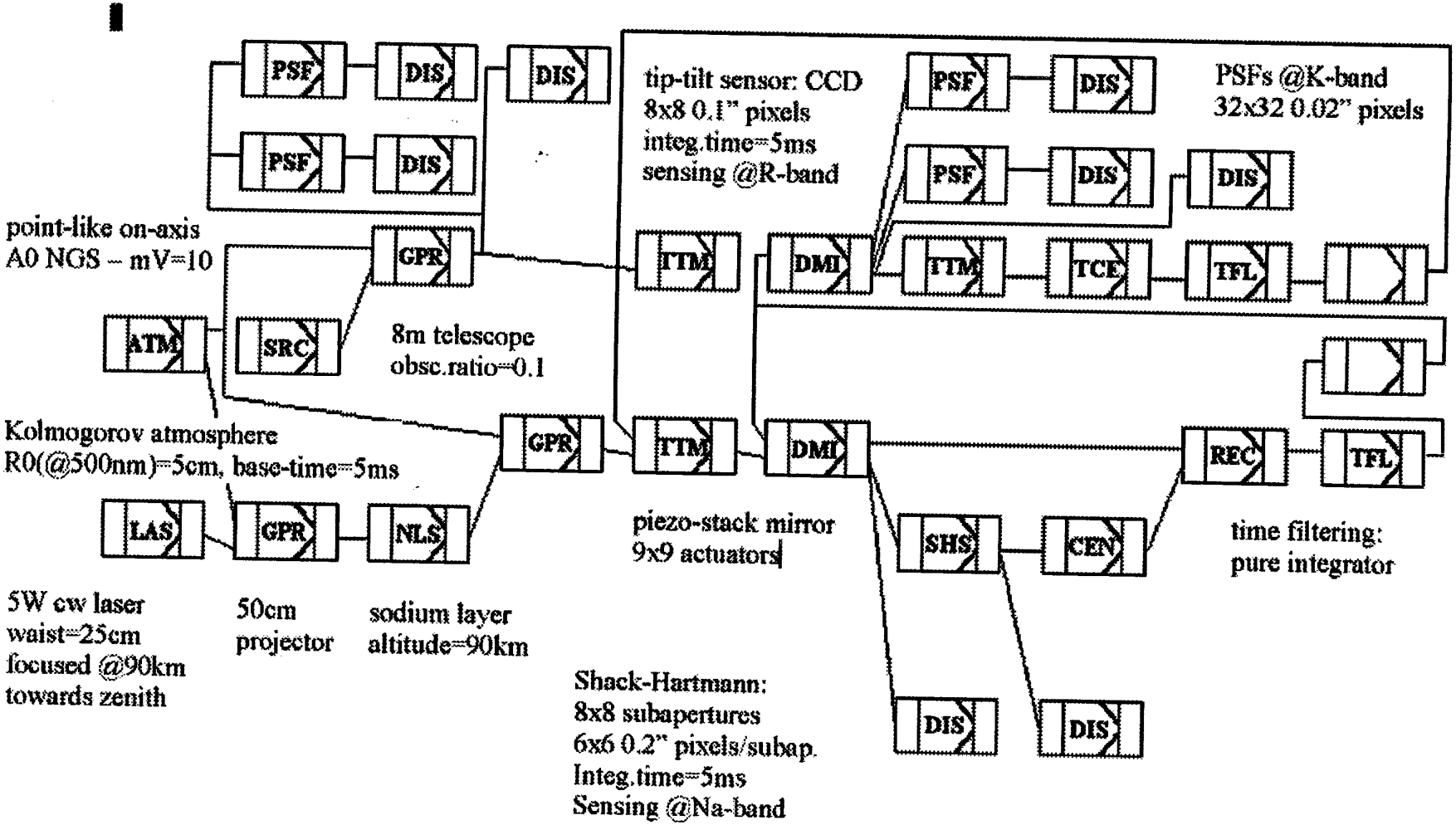
PSF
DIS
DIS
PSF
DIS
point-like on-axis
A0 NGS – mV=10
GPR
ATM
SRC
8m telescope
obsc.ratio=0.1
Kolmogorov atmosphere
R0(@500nm)=5cm, base-time=5ms
LAS
GPR
NLS
5W cw laser
waist=25cm
focused @90km
towards zenith
50cm
projector
sodium layer
altitude=90km
tip-tilt sensor: CCD
8x8 0.1" pixels
integ.time=5ms
sensing @R-band
TTM
GPR
TTM
piezo-stack mirror
9x9 actuators
Shack-Hartmann:
8x8 subapertures
6x6 0.2" pixels/subap.
Integ.time=5ms
Sensing @Na-band
PSF
DIS
PSFs @K-band
32x32 0.02" pixels
PSF
DIS
DIS
DMI
TTM
TCE
TFL
DMI
SHS
CEN
DIS
DIS
REC
TFL
time filtering:
pure integrator

ATM module. The wavefront reconstruction which is performed after sensing the LGS with the Shack-Hartmann sensor was carried out taking into account only the Zernike modes ranging between 4 and 24 (within the REC module). A pure integrator was used in the TFL module (F(s)= *G/s),* the total gains of the open-loop transfer function at 0.1 Hz being 95 Hz and 159 Hz in the high order and tip-tilt adaptive loops respectively.

Notice that the GPR module appears three times: once for the NGS propagation down to the 8m observing telescope, once for the laser beam upward propagation from the 50cm projector to the Na-layer, and once for the LGS downward propagation to the 8 m observing telescope. Doing so, the 8 m observing telescope parameters have to be defined twice, as well as the parameters for the wavefront correctors (TTM and DMI). Notice the special module after the TFL module corresponding to the point where the loops are closed.

The correction was considered in the K-band ($\lambda = 2200 nm$, $\Delta\lambda = 400\ nm$) and the PSF computed both for the uncorrected and corrected cases. Figure 5 shows the resulting long-exposure PSFs, together with the diffraction-limited PSF. One can deduce from these plots that the obtained Strehl ratio is approximately 0.36. In this particular case, it is possible to form a theoretical estimate of the compensated Strehl ratio based on the contribution to the overall phase variance (see [8]). The value obtained in this way is S=0.34 agreeing closely with value obtained from the simulation.

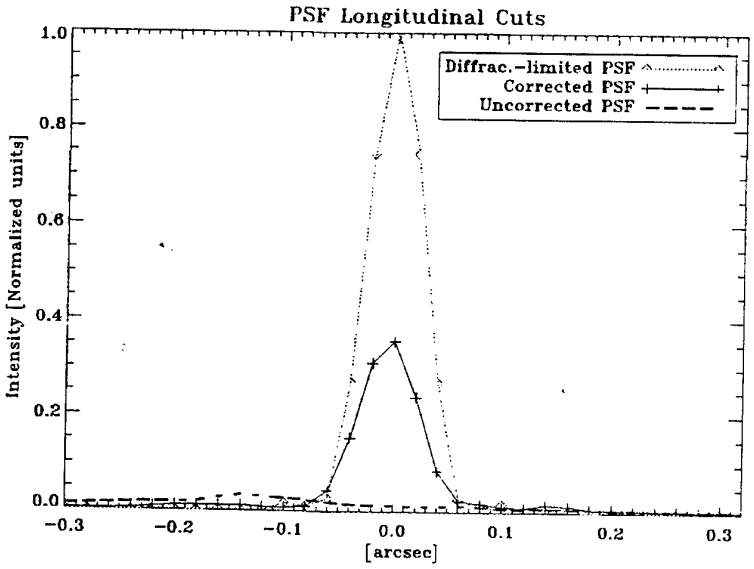

Figure 5. longitudinal cuts through the normalized PSF (uncorrected, corrected, and diffraction limited).

2. BASIS OF SIMULATION MODULES

In this section we give a brief description of the model underpinning the major modules contained in CAOS.

Wavefront Generation

Three modules are sufficient to simulate the entire process of wavefront generation as received at the pupil of the observing telescope. Implicit in this procedure is specification of the characteristics of the source (SRC module), the turbulent atmospheric model (ATM module), and the propagation from the source to the observing telescope through the atmosphere (GPR module).

2.1. Atmosphere Building (ATM) Module

The ATM (atmosphere building) module generates the turbulent atmospheric model and produces the distorted wavefronts through the module GPR (geometrical propagation). ATM therefore has no input beyond the parameters selected when the parameters setting GUI is invoked.

The output of the ATM is composed of a number of turbulent layers together with their altitudes. Each turbulent layer can be physically simulated as a random phase screen whose phase power spectrum has the von Karman or the Kolmogorov behavior. If a temporal evolution is selected, its base-time is fixed within ATM and then rules all subsequent simulation branches. In this case, each turbulent layer is also affected by a velocity vector.

The first step in building the turbulent atmosphere is to generate the phase screens that will simulate the behavior of each turbulent layer. Two methods are currently available for selection: a method based on fast-Fourier-transformation- (FFT-) with boosting of low-spatial-frequency boosting [9] and an approach based on random addition of Zernike-polynomials [10]. Details are given in the associated references.

Once the phase screens have been generated, the turbulent atmosphere is built by arranging the required number of phase screens/turbulent layers with their altitudes and taking into account the $C_n^2(h)$ profile chosen by the user. If temporal evolution is needed, this is done once only. ATM will then just shift each of the layers taking into account the base-time (minimum atmosphere/turbulence evolution time) and their associated velocity vectors. If temporal evolution is not selected , no base-time and no velocity vectors are requested and consequently each time that ATM is called, it outputs a statistically independent ensemble of turbulent layers.

2.2. Source Building (SRC) Module

A natural object or an artificial laser beacon (LGS) can be generated and in both cases they can be defined as either point-like or as an extended bidimensional object. For a natural object, the

angular coordinates of the source (off-axis and position angle), source V-magnitude (background magnitudes for any subsequent noise computations) and spectral type can be chosen via the corresponding parameter setting GUI. The flux from the natural source and the sky background are then derived for the whole range of optical Johnson bands (from U to M). The angular coordinates are passed to the GPR module with respect to a so-called main telescope having coordinates [0,0,0]. The actual telescope pointing to a given source may be distinct from this. For a LGS, its finite distance to the telescope must also be provided and the source flux (computed from its equivalent V-magnitude) is non-zero only in a narrow Na-band ($\lambda = 589\ nm$, $\Delta\lambda = 10\ nm$) .

2.3. Geometrical Propagation (GPR) Module

GPR performs geometrical propagation through the atmosphere by linear superposition of the fluctuations produced by each turbulent layer. The module can be used to simulate either downward propagation through the atmosphere (together with SRC and ATM) or propagation upwards through the atmosphere. In both cases, the simulation takes into account the physical coordinates of the two objects from which and to which the propagation has to be performed in order to establish which part of each atmospheric layer has to be used.

For natural objects located at infinity, all the wavefront portions chosen at different altitudes have the same size as the telescope pupil. Thus the light beam propagation shape is cylindrical. On the other hand, a sodium LGS is situated at a finite distance from the observing telescope and the light beam propagation shape is conical. The relevant surface for the upper layers is thus smaller than for the lower ones. This cone effect is simulated using a rescaling method. In other words, before carrying out the linear superposition, each portion of the wavefront is magnified by a factor $\frac{H_{Na}}{H_{Na} - h_i}$ where H_{Na} is the altitude of the sodium layer, and h_i, is the altitude of a given turbulent layer. The number of photons from the natural source and the sky background are computed using the value of the diameter and the obscuration ratio of the observing telescope, as well as the respective fluxes from SRC. The only parameters needed before running this module are the coordinates of the observing telescope with respect to the point [0.0.0], its diameter and the obscuration ratio.

2.4 Tip-Tilt Sensing and Correction (TTS, TCE and TTM) Modules

The TTS (tip-tilt sensor) simulates the process of imaging the wavefront coming out of the GPR module. The designer can define the number of pixels in the detector, the field of view subtended by each pixel, the algorithm to estimate the tip-tilt, the sensitive bandwidth of the detector and the integration and delay times. The module can also take into account different noise sources, namely Poisson photon and dark-current noises and Gaussian read-out noise. The intensity pattern in the focal plane is computed by using standard Fourier-based scalar diffraction theory.

In the case of tip-tilt sensing with a LGS (generated with the LAS and NLS modules) each sub-layer is treated as an extended bidimensional source, so that for each sub-layer we compute a

PSF aberrated by atmospheric turbulence plus the defocus aberration caused by the fact that the LGS is only focussed in a given plane.

In a conventional AO set-up, the TTS module is followed by a tip-tilt centroiding calculus (TCE) module that takes the intensity pattern on the detector as input and estimates the tip-tilt according to the detector and algorithm chosen. CAOS currently provides barycentre calculus for a CCD, or quadrant differential measurement for a Quad-cell detector.

The required inputs into the tip-tilt mirror (TTM) module are a GPR-propagated wavefront and a set of measurements from the TCE module. Sometimes, the designer may wish to first filter these in the time domain using the TFL module. A tilted plane is then subtracted from the wavefront in order to correct the measured tip-tilt. No dynamic behaviour of the tip-tilt mirror is explicitly considered although this is possible with a suitable choice of time filter (see next section).

2.5 Time Filtering (TFL) Module

The time filtering (TFL) module implements a recursive digital filter in the time domain. Because most AO systems work in closed loop, the TFL module can be used to emulate a servo-control law and time filter the instantaneous estimate of the residual wavefront requiring correction before applying it to the wavefront corrector. The design of the servo-control law is critical in order to ensure the closed-loop stability and provide optimal performance for a given AO system, atmospheric conditions and reference source.[20,21] The TFL module, however, is not limited to simulation of a control law and can be used whenever time filtering is needed. For example, noise filtering in open loop configuration can be simulated in this way.

The equivalent Laplace domain transfer function for the digital filter design can be selected from any of the following: (i) a generic analog filter expressed in terms of gain, zeros and poles. (ii) a single pole at zero frequency with a user defined gain G, i.e. a pure integrator with $H(s) = G/s$, and (iii) a proportional-integrator-derivative (PID) filter given by-

$$H(s) = K_p + \frac{K_I}{s} + K_d \frac{\omega_0 s}{s + \omega_0}$$

where K_p, K_I *and* K_d are the gains for the proportional, integral and derivative components of the filter, the low-pass correction term $\frac{\omega_0}{\omega_0 + s}$ with cut-off frequency is introduced to filter out the contribution of the high-frequency noise in the derivative component. In each case, the Z-transform of the corresponding digital filter is computed via use of the bilinear approximation, and the recurrence relationship is shown within the parameter setting GUI. One can also plot the Bode diagram of the equivalent analog filter. The TFL module code accepts a command type structure data as input, in which the present values of the discrete-time signals to filter are stored. The same digital filter is applied to each signal, and the result is passed in another command type structure data as output.

2.6 Shack-Hartmann Sensing (SHS) Module

The SHS module computes the image of the guide object (i.e. natural, point-like guide star, extended laser beacon etc) as viewed by each subaperture of the Shack-Hartmann lenslet array. It then combines them into the full sensor image resized to the CCD scale, integrates the images over the integration time and adds the noise. Its input is the wavefront and its output is the CCD sensor image integrated over the required time.

The Hartmann lenslet geometries may be selected from the following –

i) A square geometry.
ii) Hexagonal geometry.
iii) Radial geometry with equal area subapertures.
iv) A generalised radial geometry in which the number of rings in the array and the number of subapertures per ring may be specified
v) Customised geometry defined by means of a user-supplied file (which must contain the sensor geometry array and optical axis positions of the lenslet in this array).

The default setting is to assume that the pupil is centered on the sensor. However, the size of the pupil relative to the sensor and its relative shift can be specified if required.

CCD camera characteristics can also be specified within this module. The number of camera pixels corresponding to one subaperture, the angular size of a CCD pixel, the subaperture angular size (if there is a field stop placed in front of them), the integration time and read-out time and the working wavelength band can be set. It is also possible to consider the noises (in the same way as in the TTS module), and to use a standard Gaussian calibration fiber or a specific one (adjustable FWHM and shape). Differential elongation of LGS tridimensional spot and Rayleigh scattering cone on each subaperture have also been implemented.

An example of a simulated CCD sensor image is shown in Fig. 6 for a square 7x7 Shack-Hartmann sensor, with 8x8 pixels under each subaperture. The aberrated wavefront corresponds to third order astigmâtism.

2.7 Centroiding calculus module (CEN)

The CEN module takes the output from a SHS CCD image and defines the pixels over which the estimate of the subaperture centroid is to calculated. The calculated centroid positions can be linearly related to the local slopes of the wavefront averaged over the subapertures. One can choose to rebin the CCD camera pixels over which the centroiding is made and can set the rebin factor to any submultiple of the linear number of pixels per subaperture. One can also decide to use the fibre reference measurements as zeros for CEN output measurements or to give the raw (non-referenced) data. The extracted pixels, on which centroiding is computed, can be centred on the subaperture optical axis (usual case) or on the reference measurement central positions (useful in case of large static aberrations).

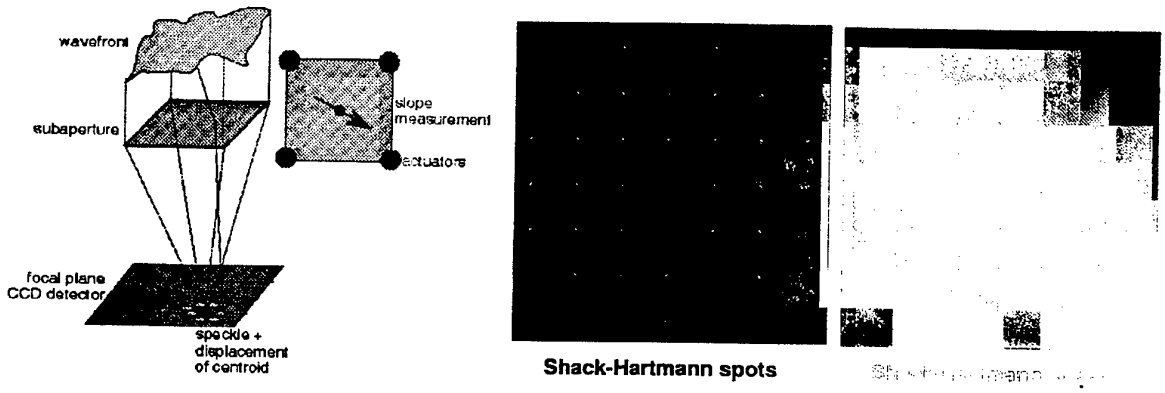

Figure 6. Shack-Hartmann wavefront sensor (left), representation of the spots (centre) and of the measured slopes (right) for a square 7x7 subaperture sensor.

2.8 Reconstruction (REC) Module

Input to the REC module is the centroiding measurements which are output by CEN. The REC module can be employed to perform three basic functions -

(i) To visualize the measured approximation of the wavefront for the Fried geometry. In this case, the output is the local wavefront phase reconstructed at the actuator positions.

(ii) To compute the mirror commands to be sent to the time filtering module. In this case, the output is the mirror command voltages.

(iii) To evaluate the modal coefficients of the measured wavefront. In this case, the output of the module is the modal coefficients of the specified basis functions. Any of the three bases: mirror modes, Zernike circular polynomials or a Karhuenen-Loeve basis may be specified. The interaction matrix can be automatically calibrated by the simulation or can be provided by the user. Command-to-mode and mode-to-command transfer matrices are also computed from the mirror influence functions.

2.9 Deformable Mirror (DMI) Module

The DMI module builds the deformable mirror geometry as well as its influence functions, and uses the commands computed by the reconstructor and time filtering modules in closed loop to correct the incident wavefront. It therefore requires two inputs: the incident wavefront to be corrected and the commands coming from the reconstruction (REC) or time filtering (TFL) module. DMI has two outputs: the corrected wavefront and the mirror geometry parameters needed by the reconstructor module to build the interaction and passage matrices (number of active actuators and influence functions of the mirror). One can specify the geometry of the mirror, its influence function characteristics, and its dynamic behavior. If required, one can also

specify the size and central shift of the pupil on the mirror, the angle of incidence of the wavefront and the mirror azimuth angle in its own plane relative to the plane of incidence.

Currently, 2 pre-defined piezo-stack mirror geometries are provided. These are square and rectangular geometries with the number of actuators and spacing along x- and y-axes specified by the user. A custom geometry can also be defined. The dynamical behavior of the actuators is characterized by the gain (displacement induced by a unit voltage command), by the maximum admissible actuator stroke and by the time delay between reception of the command and application of the stroke. Hysteresis is not currently modelled.

2.10 Data analysis-system performance

Whilst the aim of CAOS is not to provide extensive data analysis tools, basic system performance is provided through the following modules –

PSF - a point spread function/image computation module
DIS - a generic data display module
SAV - for saving data generated during the simulation
STF - a structure function computation module

The specific functionality of these modules can be found in the user documentation.

2.11 CAOS – CONCLUSION

Our experience to date has shown that CAOS is a powerful tool for the simulation of adaptive optics systems enabling studies of scientific issues to be carried out with much less effort than would be required by writing one's own code.

Particularly attractive features are i) There is no need for the user to get involved in low level coding ii) The well-defined and clear use of modules enabling simple modeLling and design iii) In those cases where CAOS cannot provide the required functionality, the user may contribute their own module provided it follows the established protocol (though this has not been carried out in our case). Disadvantages of the CAOS approach in our experience are i) The overall flexibility means that the generated code is not optimized. Execution time can be long and it is demanding on computer memory resources (in general, 128 Mbytes Ram should be considered a minimum). ii) The software is not as stable as would be ideal.

In conclusion, however, we believe that CAOS ranks as an excellent tool for AO studies. It's continued development and improvement and more widespread use should mean that it will become an increasingly important resource for the AO community.

References

1. R. Foy and A. Labeyrie, "Feasibility of adaptive telescope with laser probe," *Astron. Astrophys.* **152,** pp. L29-L31, 1985.
2. L. M. Le N. Hubin, R. Foy, and M. Tallon, "Sky coverage and PSF shape with LGS AO on 8-m telescopes," in *Adaptive Optical System Technologies,* D. Bonaccini and R. K. Tyson, eds., *Proc. SPIE* **3353,** pp. 364-370, 1998.
3. C. E. Max, K. Avicola, J. M. Brase, H. W. Friedman, H. D. Bissinger, J. Duff, D. T. Gavel, J. A. Horton, R. Kiefer, J. R. Morris, S. S. Olivier, R. W. Presta, D. A. Rapp, J. T. Salmon, and

K. E. Waltjen, "Design, layout and early results of a feasibility experiment for sodium-layer laser-guide-star adative optics," *J. Opt. Soc. Am. A* **11** (2), pp. 813-824,1994.

4. R. Q. Fugate, B. L. Ellerbroek, C. H. Higgins, M. P. Jelonek, W. J. Lange, A. C. Slavin, W. J. Wild, D. M. Winker, J. M. Wynia, J. M. Spinhime, B. R. Boeke, R. E. Ruane, J. F. Moroney, M. D. Oliker, D. W. Swindle, and R. A. Cleis, "Two generations of laser-guide-star adaptive-optics experiments at the starfire optical range," *J. Opt. Soc. Am. A* **11** (1), pp. 310-324,1994.
5. M. Tallon and R. Foy, "Adaptive telescope with laser probe: isoplanatism and cone effect," *Astron. Astrophys.* **235,** pp. 549-557,1990.
6. R. Foy, A. Migus, F. Biraben, G. Grynberg, P. R. McCullough, and M. Tallon, "The polychromatic artificial sodium star: a new concept for correcting the atmosphere tilt," *Astron. Astrophys. Suppl. Ser. III,* pp. 569-578, 1995.
7. LAOS: "A Software Package for Laser Guide Star Adaptive Optics Systems" M. Carbillet, B. Femenia, F. Delplancke, S. Esposito, L. Fini, A. Riccardi, E. Viard, N. Hubin, and F. Rigaut.
8. D. G. Sandler, S. Stahl, J. R. P. Angel, M. Lloyd-Hart, and D. McCarthy, "Adaptive optics for diffraction-limited infrared imaging with 8-m telescopes," *J. Opt. Soc. Am. A* **11** (2), pp. 925-945, 1994.
9. R. G. Lane, A. Glindeman, and J. C. Dainty, "Simulation of a Kolmogorov phase screen," *Waves in Random Media* **2,** pp. 209-224, 1992.
10. N. Roddier, "Atmospheric wavefront simulation using zernike polynomials," *Opt. Eng.* **29,** pp. 1174-1180,1990.

3. Modal wavefront projection functions with minimum error norm

In this following section, we present an article submitted for publication on June 8th 2000 to JOSA A. The paper is a theoretical contribution which shows that we may derive vector polynomials to effectively restore orthogonality to the representation of wavefronts as a modal expansion when the wavefront sensing technique provides measurement of the local gradients of the wavefront. A variational formulation shows that the polynomials are optimum as they will guarantee that the error propagation in the wavefront reconstruction is minimum. We anticipate that this subject may be of relevance to many workers in the fields of wavefront sensing, adaptive optics and optical testing.

VARIATIONAL SOLUTION FOR MODAL WAVEFRONT PROJECTION FUNCTIONS OF MINIMUM ERROR NORM

Christopher J. Solomon

School of Physical Sciences, University of Kent, Canterbury CT2 7NR, U.K.

Tel: 00-44-1227-823270

Gary C. Loos

Air-Force Research Laboratories, Kirtland Air-Force base, Albuquerque, NM 87117-6008, U.S.A.

Susana Rios

Area de Optica, Dto de Fisica Applicada, Univ. Santiago de Compostela, E-15706 Compostela, Galicia, Spain

ABSTRACT

Common wavefront sensors such as the Hartmann or curvature sensor provide measurements of the local gradient or Laplacian of the wavefront. Expression of wavefronts in terms of a set of orthogonal basis functions thus generally leads to a linear wavefront estimation problem in which modal cross-coupling occurs. Auxiliary vector functions may be derived which effectively restore the orthogonality of the problem and enable the modes of a wavefront to be independently and directly projected from slope measurements. Using variational methods, we derive the necessary and sufficient condition for these auxiliary vector functions to have minimum error norm. For the specific case of a slope-based sensor and a basis set comprising the Zernike circular polynomials, these functions are precisely the Gavrielides functions.

1. INTRODUCTION

In problems of wavefront estimation, it is common to expand the wavefront in terms of a set of orthogonal functions or modes -

$$\varphi(\mathbf{x}) = \sum_{k=1}^{N} a_k P_k(\mathbf{x}) \tag{1.1}$$

which obey the orthogonality relation –

$$\int_D P_j(\mathbf{x}) P_k(\mathbf{x})\, d^2x = \delta_{jk} \tag{1.2}$$

and D denotes the domain of integration.

The most commonly used set of functions in optics is the Zernike circular polynomials. Speaking generally, orthogonal bases are desirable because they allow the modal coefficients to be evaluated by simple integration of a product of two functions over the domain, D using the orthogonality relation given by eq. 1.2. However, since Hartmann sensors (and shearing interferometers) provide estimates of the *gradient of the phase* rather than the phase itself, the appropriate model is –

$$\left\langle \nabla\varphi(\mathbf{x}_j) \right\rangle = \sum_{k=1}^{N} a_k \left\langle \nabla P_k(\mathbf{x}_j) \right\rangle \tag{1.3}$$

where the coordinates $\mathbf{x}_j$ denote the position of the slope measurements within the pupil. In this case, the orthogonality of the wavefront basis cannot be exploited. Modal cross-coupling will occur and the coefficients must be obtained by solving an inverse problem/overdetermined system of linear equations. Many workers have examined this problem in a search for optimal solutions [1-6].

The evaluation of modes by direct integration could be restored if we can derive a set of auxiliary vector functions $\mathbf{F}_l(\mathbf{x})$ which are *orthogonal to the gradients of the basis functions.*

To establish the necessary conditions for such a set to exist, consider that the divergence of these vector functions gives the basis functions i.e. we have the relation -

$$\nabla \cdot \mathbf{F}_i(\mathbf{x}) = P_i(\mathbf{x}) \tag{1.4}$$

Using the orthogonality relation eq. 1.2 in eq. 1.1 and substituting for $P_i(\mathbf{x})$ in eq. 1.4, the modal coefficients are given by –

$$a_i = \int_D \varphi(\mathbf{x})\, \nabla \cdot \mathbf{F}_i(\mathbf{x})\, d^2x \tag{1.5}$$

This may be written as –

$$a_i = \int_D \nabla \cdot \{\mathbf{F}_i(\mathbf{x})\varphi(\mathbf{x})\}\, d^2x - \int_D \nabla\varphi(\mathbf{x}) \cdot \mathbf{F}_i(\mathbf{x})\, d^2x \tag{1.6}$$

Applying the divergence theorem, we obtain -

$$a_i = \int_D \varphi(\mathbf{x})\ \mathbf{F}_i(\mathbf{x}) \cdot d\mathbf{l} - \int_D \nabla\varphi(\mathbf{x}) \cdot \mathbf{F}_i(\mathbf{x})\, d^2x \tag{1.7}$$

Clearly if the required set of functions $\mathbf{F}_i(\mathbf{x})$ satisfies the relations -

$$\begin{aligned} &\nabla \cdot \mathbf{F}_i(\mathbf{x}) = P_i(\mathbf{x}) \\ &\mathbf{F}_i(\mathbf{x}) \cdot d\mathbf{l} = 0 \end{aligned} \tag{1.8}$$

where $\mathbf{F}_i(\mathbf{x}) \cdot d\mathbf{l}$ denotes the normal component of the function to the closed contour C of the integration domain D, we then have -

$$a_i = -\int_D \nabla\varphi(\mathbf{x}) \cdot \mathbf{F}_i(\mathbf{x})\, d^2x \tag{1.9}$$

In other words, we may evaluate the modes by *direct integration* as required. It has been shown that there are, in fact, a number of possible sets of vector polynomials which may be used in eq. 1.9 [7-9] and there is no unique solution to the problem described by eq. 1.8.

2. VARIATIONAL FORMULATION

In the remainder of this paper, we will address the question of how to derive the optimum set of vector functions $\mathbf{F}_i(\mathbf{x})$. By optimum, we mean that set of vector functions which will give the minimum error or noise propagation in our estimate of the wavefront given by eq. 1.9.

The estimate of the k^{th} modal coefficient of the wavefront will be given in practice by -

$$\hat{a}_k = \int_D \mathbf{d}(\mathbf{x}) \cdot \mathbf{F}_k(\mathbf{x})\, d^2x \tag{1.10}$$

where $\mathbf{d}(\mathbf{x}) = \nabla\varphi(\mathbf{x}) + \nu(\mathbf{x})$ and $\nu(\mathbf{x})$ is the additive noise vector at x.

If we may assume a noise process having zero mean and covariance $\sigma^2\delta(\mathbf{x}-\mathbf{x}')$ (which is reasonable for Hartmann-type sensors), it is straightforward to show that the variance in radians^2 associated with our estimate of the k mode is

$$N(\mathbf{F}_k) = \sigma^2 \int_D \left|\mathbf{F}_k(\mathbf{x})\right|^2 d^2x \qquad (1.11)$$

The noise propagator is thus defined as $N(\mathbf{F}_k) = \int_D \left|\mathbf{F}_k(\mathbf{x})\right|^2 d^2x$ and depends *only* on the particular choice of the vector functions through the volume defined by $\left|\mathbf{F}_k(\mathbf{x})\right|^2$ in D. The ensemble-averaged mean-square error associated with the estimator is then -

$$s^2 = \sigma^2 \sum_{k=1}^{M} N(\mathbf{F}_k) + \sum_{k=M+1}^{\infty} \left\langle (a_k - \bar{a}_k)^2 \right\rangle$$

where the latter term simply corresponds to unestimated modes. As the conditions specified in eq. 1.8 do not determine a unique solution for $\mathbf{F}_k(\mathbf{x})$, there are many possible solutions for each mode, each having a different associated noise propagator. The key point is that we seek to minimise the noise propagators expressed by eq. 1.10 subject to the constraint equation and boundary condition expressed by eq. 1.8. This is a variational problem. Accordingly, we introduce the Lagrange multiplier function $\lambda_k(\mathbf{x})$ and seek to minimise an objective function given by -

$$Q = \int_D \left|\mathbf{F}_k(\mathbf{x})\right|^2 d^2x + \int_D \lambda_k(\mathbf{x})\left\{\nabla\cdot\mathbf{F}_k(\mathbf{x}) - P_k(\mathbf{x})\right\}d^2x \tag{1.12}$$

We now take first variations in Q with respect to $\mathbf{F}_k(\mathbf{x})$ and set these to zero to find the stationary points of Q –

$$Q = 2\int_D \delta\mathbf{F}_k(\mathbf{x})\cdot\mathbf{F}_k(\mathbf{x})d^2x + \int_D \lambda_k(\mathbf{x})\nabla\cdot\delta\mathbf{F}_k(\mathbf{x})d^2x = 0 \tag{1.13}$$

Since $\nabla\cdot\left\{\lambda_k(\mathbf{x})\mathbf{F}_k(\mathbf{x})\right\} = \lambda_k(\mathbf{x})\nabla\cdot\mathbf{F}_k(\mathbf{x}) + \mathbf{F}_k(\mathbf{x})\cdot\nabla\lambda_k(\mathbf{x})$, this may be expressed as -

$$Q = 2\int_D \delta\mathbf{F}_k(\mathbf{x})\cdot\mathbf{F}_k(\mathbf{x})d^2x + \int_D \nabla\cdot\left\{\lambda_k(\mathbf{x})\delta\mathbf{F}_k(\mathbf{x})\right\}d^2x - \int_D \lambda_k(\mathbf{x})\delta\mathbf{F}_k(\mathbf{x})\cdot d\mathbf{l} = 0 \tag{1.14}$$

Applying the divergence theorem to the second integral in eq. 1.14 and rearranging we obtain –

$$Q = \int_D \left\{2\mathbf{F}_k(\mathbf{x}) - \nabla\lambda_k(\mathbf{x})\right\}\cdot\delta\mathbf{F}_k(\mathbf{x})d^2x + \int_C \delta\mathbf{F}_k(\mathbf{x})\cdot\lambda_k(\mathbf{x})d^2x = 0 \tag{1.15}$$

The boundary condition $\mathbf{F}_k(\mathbf{x})\cdot d\mathbf{l} = 0$ from eq. 1.8 ensures that the last integral in eq. 1.15 is identically zero and we arrive at the simple condition for the $\mathbf{F}_k(\mathbf{x})$ to have minimum error norm -

$$\mathbf{F}_k(\mathbf{x}) = \nabla\lambda_k(\mathbf{x}) \tag{1.16}$$

In other words, the $\mathbf{F}_k(\mathbf{x})$ are an *irrotational* set of functions - i.e. must be expressible as the gradient of an associated scalar function. Note we have dropped the factor of 2 as this will have no effect on the functional form. Substituting eq. 1.16 into the constraint given by eq 1.8 we find that the associated scalar field is determined by the Poisson equation with Neumann boundary condition –

$$\begin{aligned} \nabla^2\lambda_k(\mathbf{x}) &= P_k(\mathbf{x}) \qquad \mathbf{x}\in D \\ \nabla\lambda_k(\mathbf{r})\cdot\mathbf{n}(\mathbf{r}) &= 0 \qquad \mathbf{r}\in C \end{aligned} \tag{1.17}$$

This is the main result of our analysis. *The Poisson equation with Neumann boundary conditions has a unique solution and the minimum error norm, modal projector functions can be obtained by solving eq. 1.17 for the given set of basis functions,* $P_k(\mathbf{x})$. Such a set of functions was, in fact, explicitly derived in analytic form for the Zernike circular polynomial basis by Gavrielides in 1982 [10] although the noise propagation behaviour of these functions was not addressed in his original work. For completeness, their analytic form is given here -

The Gavrielides vector polynomials are defined in polar coordinates as follows –

$\mathbf{F}_i(r,\vartheta) = F^i_r(r,\theta)\,\hat{\mathbf{r}} + F^i_\vartheta(r,\theta)\,\hat{\vartheta}$ where

For $m \neq 0$

$$F^i_r = \frac{1}{\pi}\sqrt{2(n+1)}\,T^m_n(r)\cos(m\vartheta) \qquad \textit{if } i \textit{ is even}$$

$$F^i_r = \frac{1}{\pi}\sqrt{2(n+1)}\,T^m_n(r)\sin(m\vartheta) \qquad \textit{if } i \textit{ is odd}$$

$$F^i_\theta = \frac{1}{\pi}\sqrt{2(n+1)}\,Q^m_n(r)\left[-m\sin(m\vartheta)\right] \qquad \textit{if } i \textit{ is even}$$

$$F^i_\theta = \frac{1}{\pi}\sqrt{2(n+1)}\,Q^m_n(r)\left[m\cos(m\vartheta)\right] \qquad \textit{if } i \textit{ is odd}$$

$$T_n^m(r)=\frac{1}{4}\sum_{s=0}^{\frac{n-m}{2}}\frac{C_n^m(s)(n-2s+2)}{\left(\frac{n+m}{2}-s+1\right)\left(\frac{n-m}{2}-s+1\right)}\left[r^{m-1}-r^{n-2s+1}\right]$$

$$Q_n^m(r)=\frac{1}{4m}\sum_{s=0}^{\frac{n-m}{2}}\frac{C_n^m(s)}{\left(\frac{n+m}{2}-s+1\right)\left(\frac{n-m}{2}-s+1\right)}\left[(n-2s+2)r^{m-1}-mr^{n-2s+1}\right]$$

and where

$$C_n^m(s)=\frac{-1^s(n-s)!}{s!\left(\frac{n-m}{2}-s\right)\left(\frac{n+m}{2}-s\right)}$$

For $m=0$, *we have* –

$$F_r^i(r)=\frac{1}{\pi}\sqrt{n+1}\sum_{s=0}^{\frac{n}{2}}\frac{-1^s(n-s)!\ r^{n-2s+1}}{s!\left[\left(\frac{n}{2}-s\right)!\right]^2(n-2s+2)}$$

$$F_\vartheta^i(r)=0$$

(1.18)

3. CONCLUSION

Given the inherent simplicity of modal projection from slope measurements according to eq. 1.7, one may speculate that these functions should see more widespread use in wavefront sensing and estimation problems. We anticipate that the knowledge of their minimum noise propagation behaviour will make them a simple and attractive approach to wavefront estimation from slope measurements and lead to their increasing use.

It is interesting to note that the problem we have discussed of obtaining a set of auxiliary vector functions which gives minimum wavefront error norm has a close analogy with minimum physical principles. Eq.1.17 may in fact be identically used to describe the equilibrium shape of a membrane (with fixed boundary described by the closed contour C) over which a force $P_k(\mathbf{x})$ acts to produce vertical displacement

$\lambda_k(\mathbf{x})$. In this case, $\int_D |\mathbf{F}_k(\mathbf{x})|^2 d^2x$ represents the potential energy stored in the membrane and will be equal to the work done in bringing the membrane to it's equilibrium position $\int_D P_k(\mathbf{x})\lambda_k(\mathbf{x})d^2x$ only in the case of conservative fields - i.e. when $\mathbf{F}_k(\mathbf{x}) = \nabla\lambda_k(\mathbf{x})$ [11].

Acknowledgements

The authors would like to acknowledge the support provided for this work by the European Office of Aerospace Research and Development (SPC-98-4050) and the Engineering and Physical Sciences Research Council, U.K. (GR/L26339).

References

[1]. W.H. Southwell, J. Opt. Soc. Am., Vol 70. No. 8. (1980)

[2]. R.H. Hudgin, J. Opt. Soc. Am., Vol 67, 375-378, (1977)

[3]. J. Herrmann, J. Opt. Soc. Am., Vol 70, 28-35, (1980)

[4]. D.L. Fried, J. Opt. Soc. Am.,Vol 67, 370-375, (1977)

[5] E.P. Wallner, J. Opt. Soc. Am., 73 (1983) 1771

[6] C.J. Solomon, J.C. Dainty and N.J. Wooder, Optical Review 2 (1995) 217.

[7] E. Acosta, S. Bara, M.A. Rama and S. Rios, Opt. Lett. 20 (1995) 1083.

[8] S. Bara, S. Rios and E. Acosta, J. Opt. Soc. Am A 13 (1996) 1467.

[9] S. Rios, E. Acosta and S. Bara, Opt. Comm. 133 (1997) 443.

[10] A. Gavrielides, Opt. Lett. 7 (1982) 526.

[11] H.F. Weinberger, "A First Course in Partial Differential Equations", chapter 3, John Wiley and Sons. U.S.A. (1965)